IEEE Photonics Journal
An IEEE Photonics Society Publication

Open Access

Bio-Sensor Based on Trapped Mode All-Dielectric Metasurface Coated with Graphene Layer to Enhance Sensitivity

Volume 13, Number 3, June 2021

Xuesong Deng
Ming Fang
Xingang Ren
Zhixiang Huang, ***Member, IEEE***
Xianliang Wu, ***Member, IEEE***
Jiaming Shi

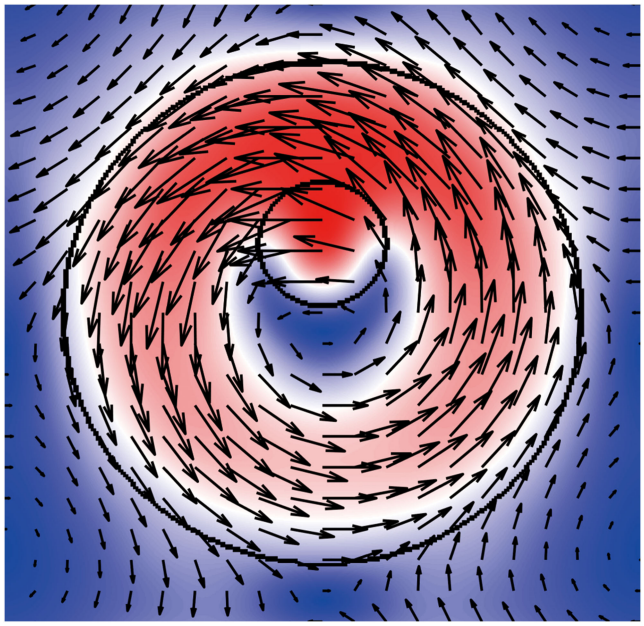

DOI: 10.1109/JPHOT.2021.3075067

IEEE photonics SOCIETY

IEEE

Bio-Sensor Based on Trapped Mode All-Dielectric Metasurface Coated with Graphene Layer to Enhance Sensitivity

Xuesong Deng,[1,2,3] **Ming Fang**,[1,2] **Xingang Ren**,[1] **Zhixiang Huang**,[1] ***Member, IEEE***, **Xianliang Wu**,[1] ***Member, IEEE***, **and Jiaming Shi**[3]

[1]Key Laboratory of Intelligent Computing and Signal Processing, Ministry of Education, Anhui University, Hefei 230039, China
[2]Anhui Province Key Laboratory of Target Recognition and Feature Extraction, Lu'an 237000, China
[3]State Key Laboratory of Pulsed Power Laser Technology, National University of Defense Technology, Hefei 230037, China

DOI:10.1109/JPHOT.2021.3075067

Manuscript received March 11, 2021; revised April 14, 2021; accepted April 20, 2021. Date of publication April 22, 2021; date of current version May 7, 2021. This work was supported in part by the National Natural Science Foundation of China (NSFC) under Grants 61901001, 61701003, U20A20164, 61971001, 61871001, and in part by Natural Science Research Foundation of Anhui Province under Grants 1908085QF259, 1808085QF179. Corresponding author: Ming Fang (e-mail: mingfang@ahu.edu.cn).

Abstract: All-dielectric metasurfaces have been widely used in nanophotonics because of their properties, such as negligible Ohmic loss, stable properties, and flexible fabrication techniques. We propose an all-dielectric metasurface consisting of subwavelength particles, which supports a "trapped" mode after the introduction of adequate symmetry-breaking in the silicon meta-atoms. Coating the metasurface with monolayer graphene enables the adsorption of nucleic acids such as DNA and RNA. We compare the resonant states in the transmission spectrum and find that the proposed metasurface is ultra-sensitive to the surrounding environment and exhibits excellent biosensing performance. Our conclusions indicate that all-dielectric metasurfaces can be a promising platform to realize ultra-sensitive bio-sensors.

Index Terms: Metasurface, bio-sensor, graphene.

1. Introduction

Metasurfaces are artificial two-dimensional materials and have attracted significant interest because of their unique electromagnetic properties, which surpass natural material properties. They are 2D counterparts of metamaterials and are capable of manipulation of light propagation. Therefore, they have been widely used in cloaking, ultra-sensitive sensors, nanolasers, and nanoantennae. Notably, metasurfaces consisting of metal have been widely explored because of their ability to confine light, which results in strong light-matter interaction. This intense light concentration can be utilized for the development of refraction index sensing [1].

High-sensitivity sensors based on the combination of metamaterials and graphene have also been actively reported [2]–[4]. However, the plasmonic metasurfaces inevitably suffer from severe

obstacles in realizing highly sensitive detection, particularly when operating at visible and infrared wavelengths [5], [6]. For instance, metal-based metasurfaces usually have very complex shapes, and there are significant technical problems associated with fabrication at the nanometer scale. Another serious issue is the intrinsic Ohmic losses at optical frequencies. The increase in parasitic absorption can induce a significant thermal effect, significantly altering the measured properties of objects and even destroying their structures [7], [8]. Additionally, for nanoscale plasmonics, metal surfaces are easily oxidized, substantially changing the resonant mode and sensing properties. This induces a broadened resonant peak, reduces the sensitivity, and limits the practical application of the entire sensory system.

A promising method to mitigate the losses and surmount the obstacles associated with metallic metasurfaces involves the concept of all-dielectric metasurfaces [9]. All-dielectric metasurfaces demonstrate several unique advantages compared with metallic metasurfaces, such as low parasitic loss, thermal stability, and flexible fabrication techniques, even for higher-frequency operation [10], [11]. In all-dielectric metasurfaces, the subwavelength dielectric meta-atoms are appropriately arranged. Each particle functions as a single resonator, maintaining a set of electrical and magnetic multipole modes called Mie-type resonances [12], which are extremely sensitive to the surrounding environment. Furthermore, the adoption of monolayer graphene on the metasurfaces can effectively enhance the organic molecular detection sensory platform's sensitivity. Graphene has several advantages: stable chemical properties, large specific surface area, and potent antioxidant capacity. The surface of single-layer graphene is easy to handle and can enhance the adhesion of organic matter, while the interlayer coupling of bilayer and trilayer graphene, whose surface is not easy to handle, which reduces the detection sensitivity. Besides, nucleic acid inclusions can be effectively absorbed on the graphene surface through the π-π stacking interaction of the hexagonal carbon ring structure and organic molecular carbon-based ring structure [13], [14]. These resonant particles generally have simple geometric shapes that make fabrication at the nanoscale easy. Thus, all-dielectric metasurfaces integrated with graphene have promising applications in the field of biological and chemical sensors.

Currently, among the various available metasurface designs, structures with strong resonance responses generated by trapped mode excitation are of particular interest. This mode has also been referred to as the "dark" state [15]–[17]. The excitation of the trapped mode is caused by the asymmetry of the subwavelength particle structure. The degree of asymmetry determines the intensity of electromagnetic coupling between the incident field and the current generated by the electric field inside the metasurface particle. Each particle serves as an independent dielectric resonator, whereas their antiphase displacement current can induce strong electromagnetic coupling within the system. The excitation of the trapped mode induces a highly confined electromagnetic field within the metasurface and produces an intense resonance. Coating the metasurface with graphene leads to the loss of a fraction of the electromagnetic energy due to graphene parasitic absorption; however, it enhances the specific resonance peak intensity by mode coupling between graphene and the dielectric resonator. Additionally, the graphene layer effectively promotes the adsorption of the analyte, thereby increasing the detection sensitivity [18]–[20].

In this article, we propose an all-dielectric metasurface consisting of subwavelength particles, which supports the "trapped" mode after introducing adequate symmetry-breaking in silicon meta-atoms. By integrating the metasurface with monolayer graphene, the combined nanostructure enables the adsorption of nucleic acid inclusions such as DNA and RNA [21]. We compare the resonant state in the transmission spectrum and find that the proposed metasurface-based platform is ultra-sensitive to the surrounding environment and exhibits excellent bio-sensing performance. Our study demonstrates that the particles in the metasurface serve as independent dielectric resonators, supporting a set of electrical and magnetic modes [22]. The proposed hybrid structure reveals that the all-dielectric metasurfaces coated with graphene have natural advantages for sensory applications.

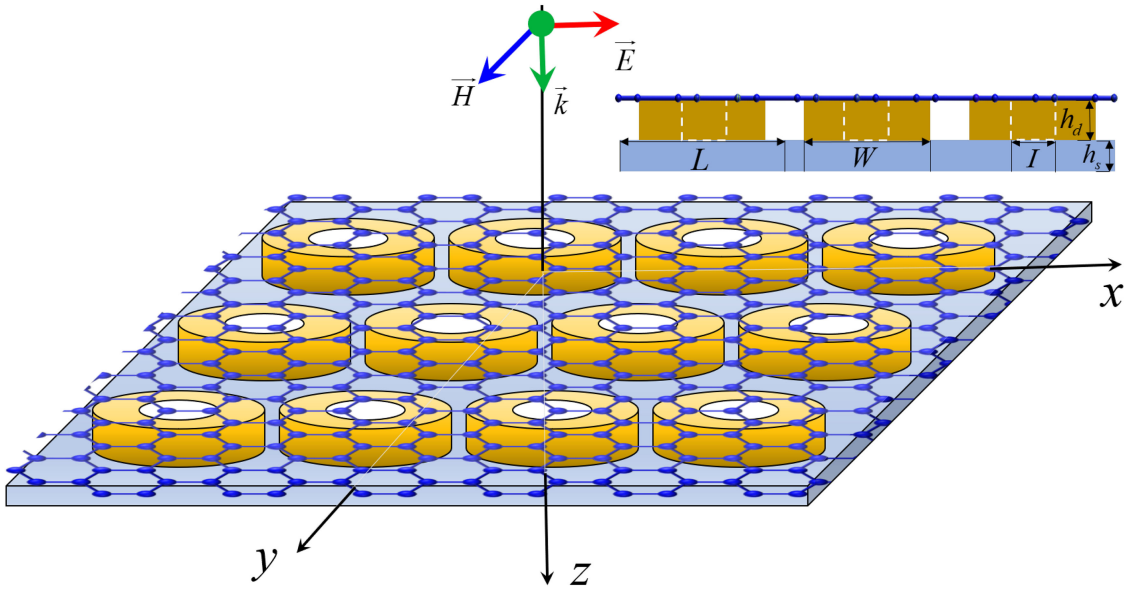

Fig. 1. Fragment of an all-dielectric metasurface with monolayer graphene. Particles have a cylindrical eccentric penetration hole, and the entire particle array is placed on the dielectric layer. The left inset illustrates the details of the cross-sectional-view of the xoz plane, and the right inset shows the top view of the unit cell. The entire structure is generally exposed to incident electromagnetic waves along the x-component of the electric field vector $\vec{E}$.

2. Design and Simulation

The designed metasurface can be regarded as a collection of open volumetric dielectric resonators with a unified structure. The electromagnetic response of an individual resonator is the same as that of the overall metasurface collective resonance, but the latter becomes considerably stronger than that of a single resonator [20]. Generally, increasing the volume of a dielectric resonator or using optical materials with a high refractive index (RI) for metasurface fabrication can be used to decrease the operating frequency of a resonator effectively. According to the metamaterials theory [10], the size of a single resonator must be smaller than the wavelength of the incident wave; therefore, materials with high contrast should be used to manufacture a metasurface that operates in near-infrared light.

We study a metasurface consisting of cylindrical silicon particles that are periodically arranged in the *xoy* plane. The lattice size is the same in both x- and y- directions, i.e., $L_x = L_y = L$. The dielectric metasurface is sandwiched between a monolayer graphene sheet and a SiO2 substrate. The diameter of the silicon meta-atom is W, and the thickness is h_d (the left inset in Fig. 1 illustrates the details of the cross-sectional view). Unlike the use of solid cylindrical particles, the off-centered round air hole is introduced in each silicon lattice, where the diameter of the air hole is set as I and the height is h_d. The off-centered air hole shifts along the y-axis in the negative direction by a distance δ to produce the appropriate asymmetry (the right inset in Fig. 1 illustrates a top view of the unit cell).

Thus, the silicon meta-atom exhibits asymmetry relative to the lines drawn through their center parallel to the *x*-axis, whereas it is still symmetrical along the *y*-axis. The silicon materials are magnetically lossless with a permittivity of $\varepsilon_d = 12.11$, and the monolayer graphene-coated on the cylindrical array of the silicon particles has a thickness of 0.34 nm[22]. The thin quartz substrate (thin relative to the wavelength of an incident wave) with a permittivity of $\varepsilon_s = 2.19$ and thickness $h_s = 100$ nm is located beneath the silicon layer. Finally, the monolayer graphene, silicon array, and silica substrate form an integrated metasurface.

Graphene is widely used in biological and chemical experiments because of its strong adsorption, electronegativity, stable chemical properties, and relatively excellent water solubility[13]. However, the frequency-independent intrinsic light absorption rate of monolayer graphene is 2.3%, which slightly reduces the transmission of various modes in an all-dielectric metasurface[14]. Nevertheless, the introduction of graphene into the sensory platform can significantly enhance the sensitivity of detection as a result of the π-π stacking interactions between graphene and nucleic acids. The surface conductivity of graphene has been adopted to model the monolayer graphene in simulation. According to Kubo's formula, the surface conductivity of graphene is the sum of interband and intraband contributions[18], expressed as

$$\sigma_g = \sigma\left(\omega, \mu_c, \Gamma, T\right) = \sigma_{inter}\left(\omega, \mu_c, \Gamma, T\right) + \sigma_{intra}\left(\omega, \mu_c, \Gamma, T\right) \tag{1}$$

where ω is the angular frequency, μ_c is the chemical potential, Γ is the scattering rate, and T is the temperature, which is specified in the range of 300 K to 390 K in our study. When $\mu_c \gg k_B$, where k_B is the Boltzmann constant, the graphene interband and intraband terms can be approximately expressed as:

$$\sigma_{inter}\left(\omega, \mu_c, \Gamma, T\right) = \frac{-iq^2}{4\pi\hbar} \ln\left[\frac{2\mu_c - (\omega - i2\Gamma)\hbar}{2\mu_c + (\omega - i2\Gamma)\hbar}\right] \tag{2}$$

$$\sigma_{intra}\left(\omega, \mu_c, \Gamma, T\right) = \frac{-ie^2 k_B T}{\pi\hbar^2(\omega - i2\Gamma)}\left[\frac{\mu_c}{k_B T} + 2\ln\left(e^{-\mu_c/k_B T} + 1\right)\right] \tag{3}$$

where $\hbar$ is the reduced Plank constant, and q is the electronic charge. The permittivity of graphene can be presented as:

$$\varepsilon_{gra} = 1 + \frac{i\sigma_g}{\varepsilon_0 \omega \xi} \tag{4}$$

Here, ε_0 is the vacuum permittivity, and monolayer graphene has a thickness of $\xi = 0.34$ nm.

The graphene layer is patterned on top of the silicon array to ensure that the sensing dielectric film containing biomolecules can have immediate contact with the graphene. An incident wave irradiates the metasurface from the top with the component along the *x*-axis. The wavelength at transmission resonance can be expressed as [26]:

$$\lambda_p = \mathrm{Re}\left(\frac{2ic\eta\varepsilon_0 W\left(\varepsilon_{r1} + \varepsilon_{r2}\right)}{\sigma_g}\right) \tag{5}$$

where λ_p is the resonance wavelength of the graphene film, c is the velocity of light in a vacuum, L is the width of the unit cell, and ε_{r1} and ε_{r2} are the permittivities of the fillers above and under the graphene, respectively. η is a dimensionless constant representing the electrodynamic response of the metasurface. As the surface conductivity is related to the graphene Fermi energy level (E_F, approximately equal to the chemical potential μ_c) and the wavelength of the electromagnetic wave, the resonance wavelength can be derived as given below:

$$\lambda_p \cong \sqrt{\frac{2\pi\hbar c}{q}\left(\frac{\eta\varepsilon_0 W\left(\varepsilon_{r1} + \varepsilon_{r2}\right)}{\mu_c}\right)} \tag{6}$$

Equation (6) shows that λ_p shifts with a slight change in the permittivity ε_{r1} of the detected material. Thus, the biomolecules can be detected by observing the change in resonant spectra.

There are two main parameters, i.e., the sensitivity and detection accuracy, that are used to assess the performance of a biosensor. The sensitivity (S) is defined as the ratio of the amount of change in the resonant wavelength ($\Delta\lambda_p$) to the change in RI in the sensing material (Δn_s, $n_s = \sqrt{\varepsilon_{r1}}$).

$$S = \frac{\Delta\lambda_p}{\Delta n_s} = \frac{2\pi\eta\hbar c}{q}\sqrt{\frac{\varepsilon_0 W}{\mu_c}}\frac{2n_s + \Delta n}{\sqrt{\left(n_s^2 + \varepsilon_{r2}\right)} + \sqrt{(n_s + \Delta n)^2 + \varepsilon_{r2}}} \tag{7}$$

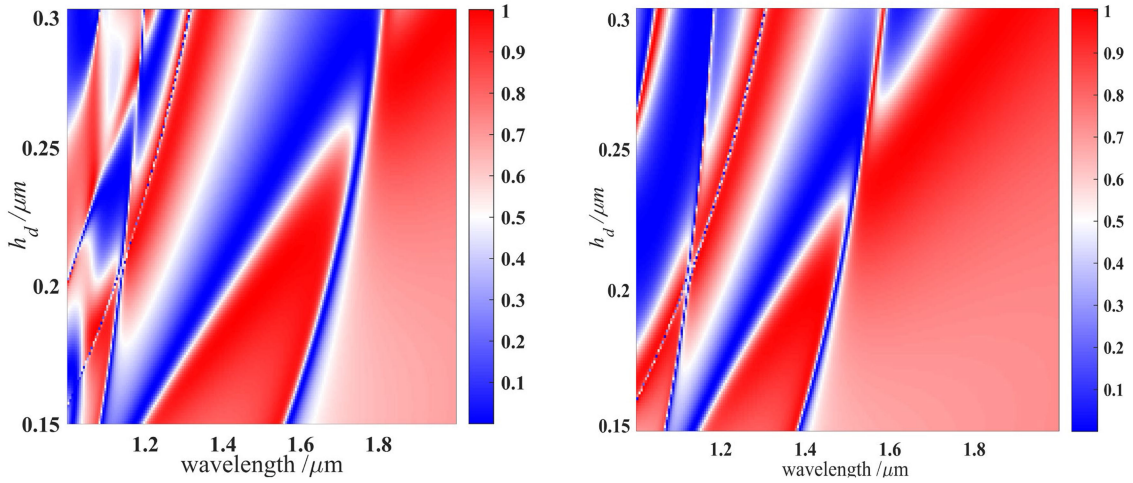

Fig. 2. Variation of transmission spectra as functions of the height of a single particle and the incident wavelength. (a) Without carved hollow and (b) with an etched hole in the center.

The detection accuracy is usually represented as the reciprocal of the full width at half-maximum (FWHM) of the resonance spectrum. The figure of merit (FOM) can comprehensively evaluate the performance of a biosensor and is defined as:

$$FOM = \frac{S}{FWHM} \tag{8}$$

The purpose of our study is to produce a unique resonance state known as the trapped mode (also known as the dark mode in reference [16]), generated when the element of a metasurface possesses specific symmetry-breaking. Therefore, we use the high-quality factor of the trapped mode and the strong adsorption of nucleic acid inclusions by graphene to design a high-performance sensor platform. The strategic design of introducing eccentric holes in surface particles usually leads to structural symmetry-breaking. In the array structure, such an asymmetry arises in the *xoy* plane along the *x*-axis (*x*-polarization). To excite the trapped mode, the vector of electric field strength $\vec{E}$ should have a nonzero component along the *x*-axis. Thus, the incident waves in our study unconditionally excite the resonance modes along the *x*-axis.

We primarily study the transmission spectra within the range of 1-2 μm to improve the accuracy of the Mie resonance-based sensor proposed above [23], [24]. We used a semi-analytical electromagnetic algorithm called rigorous coupled-wave analysis (RCWA) to study the all-dielectric metasurface's electromagnetic scattering. The variations of the transmission efficiency with the wavelength and the thickness of the silicon dielectric layer are shown in Fig. 2. By comparison of the spectra of a solid dielectric and central perforated dielectric lattices, we observed that the transmission efficiencies of the two structures reach the maximum at a thickness of 0.21 μm, which shows that the transmission efficiency between the EH_{11v} and HE_{11v} modes of the two structures are the highest. Therefore, the thickness of the silicon dielectric layer is set at 0.21 μm in the study.

3. Results and Discussion

We systematically demonstrate the resonant properties of the trapped mode in metasurfaces with symmetrical and asymmetric unit cells. The accuracy of the study is first guaranteed by simulating the electromagnetic response of a metasurface with symmetric and asymmetric inclusions in this section. Despite the structure of the particles, the resonant conditions that occurred in the metasurface rely primarily on the modal composition of individual dielectric resonators that constitute

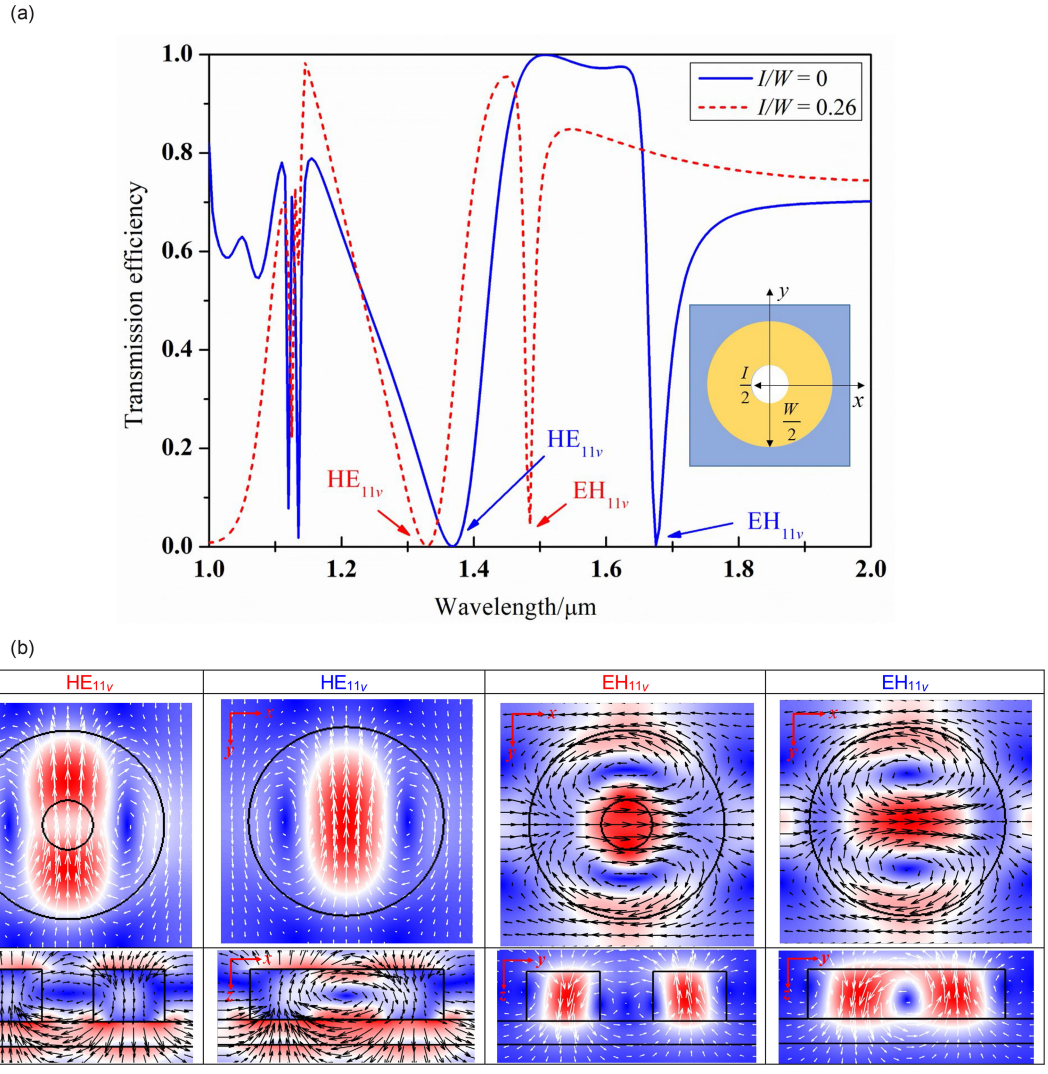

Fig. 3. (a) Transmission efficiency of two symmetrical structures. Blue solid lines represent solid particles, while red dotted lines indicate the structure with a central hole. (b) Cross-sectional patterns of electromagnetic field distribution of Mie and trapped modes at corresponding resonance frequencies for electric (black arrow) and magnetic (white arrow) fields; $h_s = 0.1\,\mu$m, $W = 0.693\,\mu$m, $l = 0.18\,\mu$m, and $L = 0.9\,\mu$m, the positions of the four resonance peaks correspond to 1.33 μm, 1.368 μm, 1.485 μm, and 1.675 μm respectively.

the metasurface, instead of the electromagnetic coupling of each dielectric resonator on the entire metasurface. Thus, we study the internal electromagnetic field mode and the distribution of the displacement electromagnetic current inside the particle at the particular resonant frequency. We use a semi-analytical algorithm that naturally correlates the resonant state of the metamaterial with the inherent electromagnetic mode of a single cylindrical resonator.

3.1. Symmetric and Asymmetric Particles

First, we calculate the electromagnetic response of a metasurface with asymmetric structure. The transmission spectra of two symmetrical structures are shown in Fig. 3(a), where the blue solid line and red denote data for a hole-free solid cylindrical dielectric block (I/W = 0) and a centrally

perforated cylindrical dielectric block (I/W $=$ 0.26) dashed line, respectively. The two resonance states are distinguished and indicated by black and white arrows at the bottom of the figure. The trough in the transmission curve denotes that the electromagnetic wave at this frequency point will be primarily reflected by the metasurface, while the peaks of the transmission curve indicate that most of the electromagnetic waves can pass through the metasurface. Because of the symmetrical properties of the metasurface, the transmission spectrum remains unchanged when the incident wave is incident from the *x*- and *y*-directions. This indicates polarization insensitivity for the incident wave. In other words, the transmission spectrum remains unchanged under a TE- or TM-polarized wave [25].

If a cylindrical air hole is introduced in the center of the single resonator, the proposed new structure can still produce a similar resonant state. The improved perforated resonator has a resonance wavelength at the corresponding resonance peak. The transmission spectrum of the perforated resonator undergoes a definite blue shift compared with that of the solid cylindrical disk. The introduction of air holes effectively reduces the permittivity of the metasurface, and the electromagnetic field strength at the corresponding peak is slightly reduced.

The hybrid modes are azimuthally dependent; for HE modes, the H_z component is relatively small compared to the E_z component. The other field components for HE modes can thus be derived from a knowledge of the E_z component only. The reverse is true for EH modes[27]. In the representation of the hybrid mode, the subscripts correspond to the amounts of change in the electromagnetic field in the azimuthal, radial, and longitudinal directions inside the resonator. In the third subscript, the index p $+$ v (p $=$ 01, ...) specifies the number of half-wavelengths along the z-axis with v $=$ (2hd $/\lambda$g $-$ p) $<$ 1, and λg is the resonant wavelength corresponding to different Mie modes for the cylindrical dielectric resonator [27]. The hole splits the magnetic field peak of the surface, which further enhances the resonance peak EH_{11v} mode. The quality factor is significantly increased because the hole at the EH_{11v} resonance peak is located precisely at the maximum of the electric field.

The cross-sectional patterns exhibited by the electric and magnetic fields in the perpendicular *xoz* or *yoz* plane and horizontal *xoy* plane are analyzed at specific frequencies. The displacement current and magnetic current distributions of the single cylindrical dielectric resonator are shown in Fig. 3(b). It can be inferred that the specific electromagnetic coupling among the linear polarized incident wave and the lowest-order (dipole) magnetic mode (first Mie resonance) and electric mode (second Mie resonance) [20] are associated with HE_{11v}-mode and EH_{11v}-mode electromagnetic resonance. It can be concluded from reference [13] that the mode of a cylindrical resonator is similar to that of a cylindrical resonator. In fact, among the parameters of the resonator, the resonant wavelength of the HE11v-mode is mainly determined by the disk height, whereas that of the EH11v-mode depends primarily on the disk radius. Therefore, these resonance modes may have different orders depending on the height and radius of the resonator.

Fig. 4(a) demonstrates the transmittance of a single dielectric disk with an asymmetric structure at two different perforation offset distances for $\delta=$ 75nm and $\delta =$ 150 nm respectively. It can be found that when the offset distance is 150nm, the resonance displacement and detection accuracy are relatively suitable through comparison; therefore,150nm is selected as the subsequent step sensor application research. The resonant state of the modified structure is similar to the previous resonant peak, but there is an additional resonant peak near 1.8 μm. An intrinsic resonance causes this resonant peak resulting from the asymmetry of the structure, and only the *x*-polarization wave can excite the trapped mode. At the EH_{11v}, TE_{01v} resonance peak, the displacement current at the *xoy* cross-section of this mode is a typical circular pattern revolving around the center of the metasurface unit cell. The circular flow generates a magnetic moment along the *z*-axis, appearing in the visible and infrared spectra. This further shows that the all-dielectric metasurface can achieve artificial magnetism, and the full resonant trap mode can be conveniently used for sensory applications, biological treatment, and other fields [28].

In the TE_{01v} resonance peak, the presence of the component parallel to the *x*-axis antiphase oscillates because of the displacement current around the particle. This produces a scattering field with very low electromagnetic coupling with the linear x-polarized incident wave, which significantly

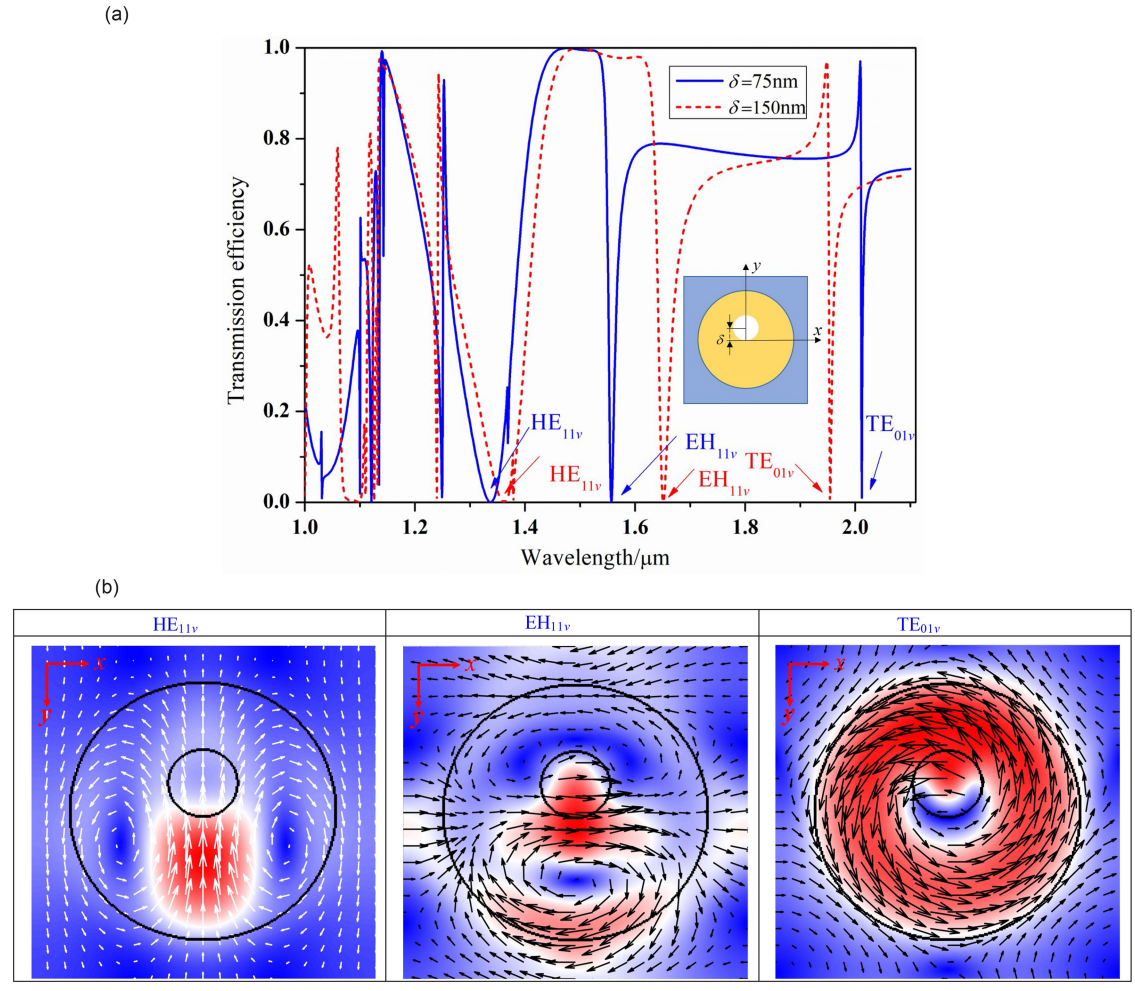

Fig. 4. (a) Transmission efficiency diagram of two asymmetric structures with different offsets. (b) Cross-sectional patterns (total field) of electromagnetic field distribution of Mie and trapped modes at corresponding resonance frequencies for electric (black arrow) and magnetic (white arrow) fields; $h_d = 0.21\,\mu$m, $h_s = 0.1\,\mu$m, $W = 0.693\,\mu$m, $l = 0.18\,\mu$m, and $L = 0.9\,\mu$m, the positions of the three resonance peaks correspond to 1.337 μm, 1.557 μm, and 2.012 μm respectively.

diminishes the radiation loss. This electromagnetic mode used to describe the weak coupling to free space is called the trapped mode. The intensity of the induced internal field strength in the trapped mode can reach an intense level, thereby ensuring a strong resonance response. The resonant peak of the trapped mode has an exceptionally high-quality factor compared with the typical Mie resonance peak.

3.2. Sensing Application

Graphene sensory platforms with asymmetric structure can be used for tumor diagnosis because they can detect tumor biomarkers such as protein, DNA, and RNA. According to the displacement of the transmission peak of the trapped mode, the metasurface structure shows higher sensitivity than conventional silver nanocrystals[21]. As a tumor suppressor, miRNAs have been found in many human cancer specimens, especially lung cancer specimens, where miRNA-21 can be used as a biomarker for the diagnosis and treatment of cancer. The structure designed in this article can rapidly detect trace amounts of miRNA-21 at low concentrations and can be used for the early

diagnosis of lung cancer [24]. It has been reported that miRNA can hybridize with the thiolated single-stranded DNA (ssDNA) molecule with a specific sequence [21].

The hybridization will significantly influence the RI of the surrounding solution such that the RI will dramatically change from 1.37 to 1.72. The increase in the RI of the structure's surface will directly cause a redshift in the various transmission peak positions, among which the redshift of the trapped mode is the most obvious. This makes it possible to detect DNA and RNA molecules with high sensitivity on metasurface particles.

The metasurface with monolayer graphene sensory platform designed here was placed in H_2O, after which ssDNA as a probe molecule was added to the solution. The ssDNA will be naturally adsorbed to the graphene surface, equivalent to the particle being covered with a dielectric layer because of the strong adsorption of graphene. A small amount of graphene oxide was added to the solution; graphene oxide possesses several functional groups that lead to combining with nucleic acid inclusions more quickly so that they can adhere to Si because of graphene oxide's electronegativity [29], [30]. This causes a slight change in the RI of the surrounding solution, leading to a redshift in the transmission peak. When a bio-extract solution containing miRNA, it will be superimposed on the metasurface; this will also increase the thickness of the organic molecular layer on the upper surface, thereby changing the RI around the top solution. In the simulation, the thickness of the ssDNA layer is set to 10 nm, and the RI is 1.57. The ssDNA and miRNA combine in 90°C solutions to form a new dielectric layer with a thickness of 20 nm and an RI of 1.72, where the RI of the solution of pure water is 1.33. The reaction process diagrams I, II, and III are shown in Fig. 5(a), and the transmission spectrum is drawn under three conditions represented by different curves in Fig. 5(b).

As shown in the transmission spectrum in Fig. 5(b), a redshift in the transmission curve occurs with a change in the RI of the upper solution, especially for the TE_{01v} peak, because the trapped mode produces great resonance accompanied by a tangential electric field that is extremely sensitive to the change in the RI. The strength of the tangential electric field produced by the EH_{11v} peak is significantly weaker than the electric field produced by the trapped mode; therefore, the redshift phenomenon caused by the trapped mode is the most apparent shift. The mode of the HE_{11v} peak produces an electric field parallel to the particle surface, which is the weakest. Therefore, the redshift effect caused by the change in RI is the lowest.

From case I to case II, the resonance wavelength λ_p of the trapped mode shifts from 1.979 μm to 2.031 μm; from case II to case III, the λ_p of the trapped mode shifts from 2.031 μm to 2.079 μm. The corresponding sensitivity (*S*) values obtained for TE_{01v} are 216 nm/RIU and 320 nm/RIU, respectively. The corresponding FOM values are 24000 RIU^{-1} and 35556 RIU^{-1}, respectively. The successful simulation of nucleic acid inclusions by the λ_p shift in the transmission spectrum exhibited higher sensitivity than that of previously reported biosensors [21], [24]. it can be found that the reported resonant peak shift of the silver-nanocrystalline biosensor [21] is about 20nm, and the sensitivity is about 83.3 nm/RIU,133. 33 nm/RIU, the corresponding quality factors are 0.1904RIU-1, 0. 3048RIU-1 respectively. Compared with the reported silver nanocrystal biosensor, the structure proposed in this article has greatly improved performance. Fig. 5(c) displays the electromagnetic field figure at the HE_{11v} peak and the electric field at the EH_{11v} peak and TE_{01v}. It can be concluded that the TE_{01v} peak has an intense circular displacement current that generates a vertical downward magnetic force and thus is extremely sensitive to changes in the surrounding environment. The cross-sectional field value patterns created by the resonance peaks in the three cases are similar; therefore, only the second case is shown here.

Although our simulation considers the near-infrared band, the measurements can be easily extended to shorter or longer wavelengths by decreasing or increasing the size of the silicon meta-atom. Such expandability to various frequencies has been experimentally demonstrated; therefore, our sensor platform has the potential to be applied in visible, infrared, or terahertz bands. Thus, with the complete development of nanophotonics, the all-dielectric graphene sensory platform of the asymmetric structure has broad applications in biosensing, biomedical, and other related fields.

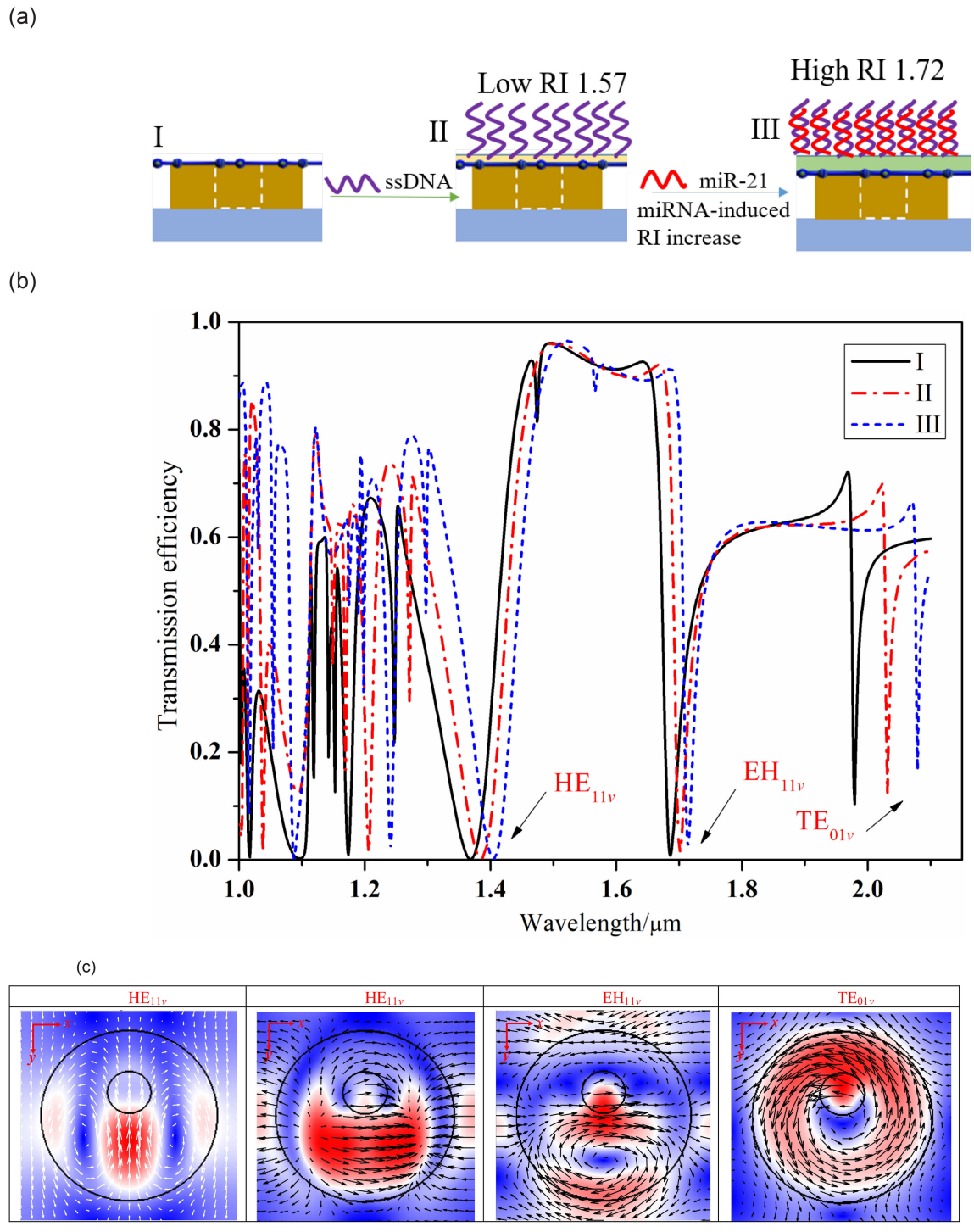

Fig. 5. (a) Three reaction process diagrams I, II, III; (b) the transmission spectrum is drawn under three conditions represented by different curves; (c) Cross-sectional patterns of electromagnetic field distribution of Mie and trapped modes at corresponding resonance frequencies for electric (black arrow) and magnetic (white arrow) fields, the three resonance peak positions of state III correspond to 1.385 μm, 1.714 μm, and 2.079 μm. respectively.

4. Conclusion

In conclusion, we demonstrate a novel platform for biosensing based on an all-dielectric metasurface engineered with monolayer graphene. This all-dielectric metasurface provides excellent sensitivity because of the sharp resonant spectrum of the trapped mode of the asymmetric meta-atom, resulting in the strong coupling between the metasurface and the test sample. Compared with biosensors based on plasmonic metamaterials, the biosensing platform that consists of silicon and graphene is more stable, sensitive, and harmless to biological samples, the sensitivity of the all-dielectric sensor designed is up to 320 nm/RIU. Besides, the operational frequency of the biosensor that corresponds to the resonant frequency of the metasurface can be flexibly tuned by scaling the dimensions of the all-dielectric meta-atom. Our observations provide a promising method to realize ultra-sensitive bio-sensors based on all-dielectric metasurfaces.

References

[1] N. Liu, M. Mesch, T. Weiss, M. Hentschel, and H. Giessen, "Infrared perfect absorber and its application as plasmonic sensor," *Nano Lett.*, vol. 10, no. 7, pp. 2342–2348, Jun. 2010.

[2] Z. Lin *et al.*, "Tuning and sensitivity enhancement of surface plasmon resonance biosensor with graphene covered Au-MoS 2-Au films," *IEEE Photon. J.*, vol. 8, no. 6, Dec. 2016, Art. no. 4803308.

[3] L. Wu *et al.*, "Sensitivity improved SPR biosensor based on the MoS_2/graphene-aluminum hybrid structure," *J. Lightw. Technol.*, vol. 35, no. 1, pp. 82–87, Jan. 2017.

[4] L. Wu *et al.*, "Sensitivity enhancement by using few-layer black phosphorus-graphene/TMDCs heterostructure in surface plasmon resonance biochemical sensor," *Sens. Actuators B Chem.*, vol. 249, pp. 542–548, Oct. 2017.

[5] R. Singh, I. Al-Naib, W. Cao, C. Rockstuhl, M. Koch, and W. Zhang, "The Fano resonance in symmetry broken terahertz metamaterials," *IEEE Trans. Terahertz Sci. Technol.*, vol. 3, no. 6, pp. 820–826, Nov. 2013.

[6] L. Cong, S. Tan, R. Yahiaoui, F. Yan, W. Zhang, and R. Singh, "Experimental demonstration of ultrasensitive sensing with terahertz metamaterial absorbers: A comparison with the metasurfaces," *Appl. Phys. Lett.*, vol. 106, no. 3, 2015, Art. no. 031107.

[7] T. Yue, Z. H. Jiang, A. H. Panaretos, and D. H. Werner, "A compact dual-band antenna enabled by a complementary split-ring resonator-loaded metasurface," *IEEE Trans. Antennas Propag.*, vol. 65, no. 12, pp. 6878–6888, Dec. 2017.

[8] Q. Fu, F. Zhang, Y. Fan, X. He, T. Qiao, and B. Kong, "Electrically tunable Fano-type resonance of an asymmetric metal wire pair," *Opt. Exp.*, vol. 24, no. 11, pp. 11708–11715, 2016.

[9] A. Krasnok, M. Caldarola, N. Bonod, and A. Alú, "Spectroscopy and biosensing with optically resonant dielectric nanostructures," *Adv. Opt. Mater.*, vol. 6, no. 5, 2018, Art. no. 1701094.

[10] X. Gui, X. Jing, and Z. Hong, "Ultrabroadband perfect reflectors by all-dielectric single-layer super cell metamaterial," *IEEE Photon. Technol. Lett.*, vol. 30, no. 10, pp. 923–926, May 2018.

[11] Y. Shuai *et al.*, "Fano-resonance photonic crystal membrane reflectors at mid- and far-Infrared," *IEEE Photon. J.*, vol. 5, no. 1, Feb. 2013, Art. no. 4700206.

[12] A. M. Lopatynskyi, O. G. Lopatynska, L. J. Guo, and V. I. Chegel, "Localized surface plasmon resonance biosensor—Part I: Theoretical study of sensitivity—Extended mie approach," *IEEE Sensors J.*, vol. 11, no. 2, pp. 361–369, Feb. 2011.

[13] J. Wang, L. Yang, Z. Hu, W. He, and G. Zheng, "Analysis of graphene-based multilayer comb-like absorption system based on multiple waveguide theory," *IEEE Photon. Technol. Lett.*, vol. 31, no. 7, pp. 561–564, Apr. 2019.

[14] X. Ren, E. I. Wei, and W. C. Choy, "Tuning optical responses of metallic dipole nanoantenna using graphene," *Opt. Exp.*, vol. 21, no. 26, pp. 31824–31829, 2013.

[15] M. Fang, N. H. Shen, E. I. Wei, Z. X. Huang, T. Koschny, and C. M. Soukoulis, "Nonlinearity in the dark: Broadband terahertz generation with extremely high efficiency," *Phys. Rev. Lett.*, vol. 122, no. 2, Jan. 2019, Art. no. 027401.

[16] W. Li, Y. Su, X. Zhai, X. Shang, S. Xia, and L. Wang, "High-Q multiple fano resonances sensor in single dark mode metamaterial waveguide structure," *IEEE Photon. Technol. Lett.*, vol. 30, no. 23, pp. 2068–2071, Dec. 2018.

[17] C. Park, V. R. Shrestha, S. Lee, and E. Kim, "Transmissive color switch tapping into a polarization-selective spectral filter," *IEEE Photon. Technol. Lett.*, vol. 26, no. 12, pp. 1235–1238, Jun. 2014.

[18] Y. Fan, Z. Wei, Z. Zhang, and H. Li, "Enhancing infrared extinction and absorption in a monolayer graphene sheet by harvesting the electric dipolar mode of split ring resonators," *Opt. Lett.*, vol. 38, no. 24, pp. 5410–5413, Nov. 2013.

[19] Y. Fan *et al.*, "Photoexcited graphene metasurfaces: Significantly enhanced and tunable magnetic resonances," *ACS Photon.*, vol. 5, no. 4, pp. 1612–1618, Feb. 2018.

[20] V. R. Tuz *et al.*, "High-quality trapped modes in all-dielectric metamaterials," *Opt. Exp.*, vol. 26, no. 3, pp. 2905–2916, Feb. 2018.

[21] L. Zhang *et al.*, "Refractive index dependent real-time plasmonic nanoprobes on a single silver nanocube for ultrasensitive detection of the lung cancer-associated miRNAs," *Chem. Commun.*, vol. 51, no. 2, pp. 294–297, Aug. 2014.

[22] V. R. Tuz, V. V. Khardikov, N. V. Sydorchuk, D. V. Novitsky, and S. L. Prosvirnin, "Recent development of conception of trapped modes in low-loss all-dielectric metamaterials," in *Proc. 47th Eur. Microw. Conf.*, 2017, pp. 484–487.

[23] T. Low, and P. Avouris, "Graphene plasmonics for terahertz to mid-infrared applications," *ACS Nano*, vol. 8, no. 2, pp. 1086–1101, Jan. 2014.

[24] N. Bontempi *et al.*, "Highly sensitive biosensors based on all-dielectric nanoresonators," *Nanoscale*, vol. 9, no. 15, pp. 4972–4980, Mar. 2017.

[25] J. Xie *et al.*, "Truly all-dielectric ultrabroadband metamaterial absorber: Water-based and ground-free," *IEEE Antennas Wireless Propag. Lett.*, vol. 18, no. 3, pp. 536–540, Mar. 2019.
[26] P. K. Maharana, P. Padhy, and R. Jha, "On the field enhancement and performance of an ultra-stable SPR biosensor based on graphene," *IEEE Photon. Technol. Lett.*, vol. 25, no. 22, pp. 2156–2159, Nov. 2013.
[27] R. K. Mongia, and P. Bhartia "Dielectric resonator antennas—A review and general design relations for resonant frequency and bandwidth," *Int. J. Microw. Millimeter-Wave Comput.-Aided Eng.*, vol. 4, no 3, pp. 230–247,Mar. 1994.
[28] H. Ren, X. G. Ren, Z. X. Huang, and X. L. Wu, "Synergetic light trapping effects in organic solar cells with a patterned semi-transparent electrode," *Phys. Chem. Chem. Phys.,* vol. 21, no. 21, pp. 11306–11312, Jan. 2019.
[29] N. Celik, W. Balachandran, and N. Manivannan, "Graphene-based biosensors: Methods, analysis and future perspectives," *IET Circuits, Devices Syst.*, vol. 9, no. 6, pp. 434–445, Dec. 2015.
[30] H. Fu, S. Zhang, H. Chen, and J. Weng, "Graphene enhances the sensitivity of fiber-optic surface plasmon resonance biosensor," *IEEE Sensors J.*, vol. 15, no. 10, pp. 5478–5482, Oct. 2015.